ACS OMEGA

Open Access

http://pubs.acs.org/journal/acsodf

Article

Fe-CP-based Catalytic Oxidation and Dissipative Self-Assembly of a Ferrocenyl Surfactant Applied in DNA Capture and Release

Ting Liu, Liwei Zhu, Chencan Li, Yang Yu, Zhuo Zhang, Huizhong Liu, Ling Wang,* and Yawen Li*

Cite This: *ACS Omega* 2024, 9, 23772−23781

Read Online

ACCESS | Metrics & More | Article Recommendations | Supporting Information

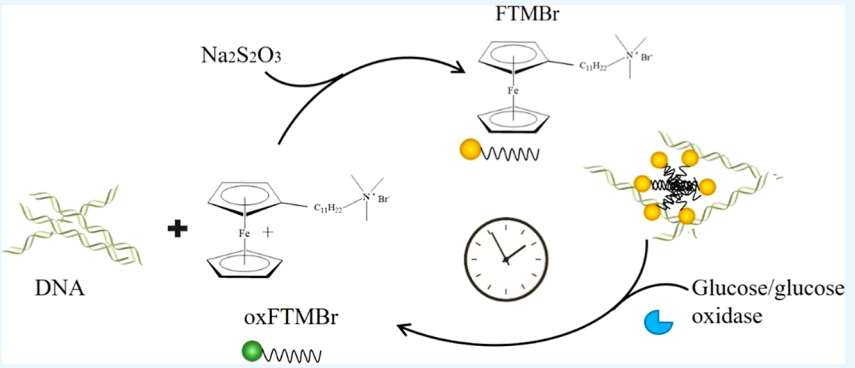

ABSTRACT: Dissipative self-assembly plays a vital role in fabricating intelligent and transient materials. The selection and design of the molecular structure is critical, and the introduction of valuable stimuli-responsive motifs into building blocks would bring about a novel perspective on the fuel driven nonequilibrium assemblies. For redox-responsive surfactants, novel methods of catalytic oxidation are very important for their activation/deactivation process through designing fuel input/energy dissipation. As an enzyme with a fast catalytic rate, Fe-based coordination polymers (Fe-CPs) are found to be highly effective oxidase-like enzymes to induce a reversible switch of a ferrocene-based surfactant over a wide range of temperatures and pH. This builds a bridge between the CPs materials and surfactants. Furthermore, glucose oxidase can also induce a switchable transition of a ferrocene-based surfactant. The GOX-catalyzed, glucose-fueled transient surfactant assemblies have been fabricated for many cycles, which has a successful application in a time-controlled and autonomous DNA capture and release process. The intelligent use of enzymes including CPs and GOX in ferrocene-based surfactants will pave the way for the oxidation of redox surfactants, which extends the application of stable or transient ferrocenyl self-assemblies.

1. INTRODUCTION

Dissipative self-assembly is ubiquitous in nature, where it gives rise to complex structures and functions such as programming controllability, self-adaptability, self-healing capability, and energy dependence. Simulating this energy-driven dissipative self-assembly in which a forward reaction activates the building blocks for self-assembly and a concurrent backward reaction brings the system back to the basal nonassembled state has attracted much attention. Elegant strategies to access non-equilibrium artificial synthetic systems have utilized molecules including peptides,[1] nucleic acid,[2] nanoparticles,[3] polymers,[4] and amphiphiles.[5] Particularly, surfactants are other amphiphiles participating in micelle or vesicle fabrication. The hydrophilic/hydrophobic structure endows surfactants with self-assembled capability, and the ways to integrate fuels into systems become the key for dissipative self-assembly. For instance, Zn(II)−TACN (1,4,7-thiazacyclonane) with hydrophobic saturated carbon chains could form temporal vesicle-like aggregates exploiting an ATP-fueled dissipative self-assembly process.[6] A double alkyl chain surfactant could fabricate vesicles through forming dynamic imine bonds between an amine-containing lysosphingomyelin and long-chain aldehydes. The reversibility of the imine is utilized to fabricate vesicles that is responsive to external stimuli.[7] It can be seen that the selection and design of the molecular structure is the critical point and the introduction of valuable stimuli-responsive motifs into surfactants would bring about a novel perspective on the fuel driven nonequilibrium assemblies.

Surfactants containing the redox active group of ferrocenyl groups have attracted great attention in the field of biophysical research.[8,9] By controlling the redox state of ferrocene, it is possible to change the charge and hydrophobicity of the

Received: February 22, 2024
Revised: April 25, 2024
Accepted: April 26, 2024
Published: May 21, 2024

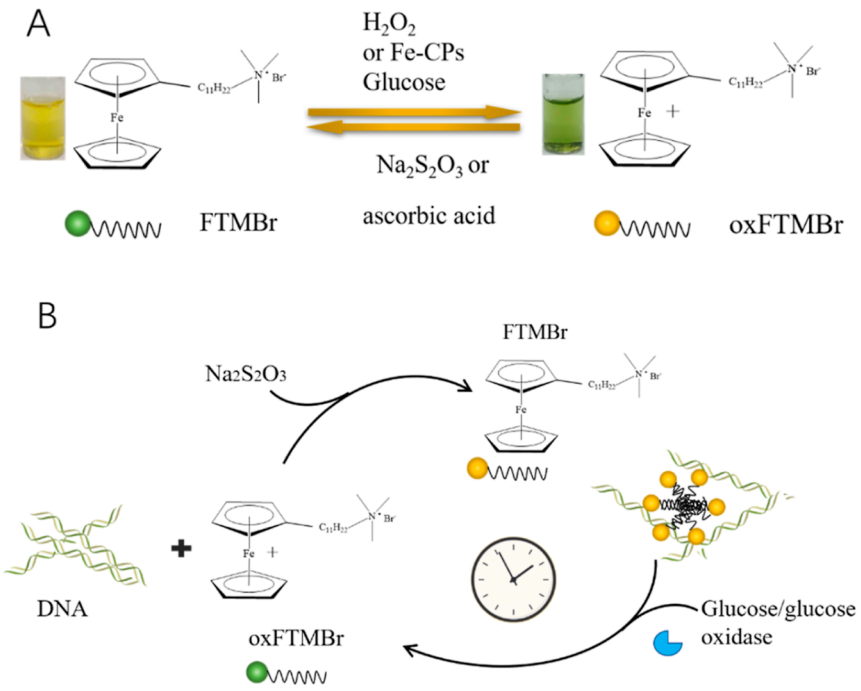

Figure 1. (A) Redox process of FTMBr with oxidizing and reducing agents. (B) Schematic illustration of GOX-catalyzed, glucose-fueled transient FTMBr micelles for controlled capture and release of DNA molecules.

surfactants, leading to a transition of the self-assembled structure.[10] Reductive ferrocenyl surfactants have the ability of self-assembling into various aggregates like micelles, vesicles and gels, while the oxidative surfactant would return to the single surfactant. Therefore, the integration of the ferrocenyl surfactant and diversity of fuel is a particularly important step in the construction of high energy and nonequilibrium redox-responsive assemblies. Dissipative self-assembly is dynamically controlled. In order to achieve the temporal assemblies, the challenge is to find a subtle balance of activation−deactivation rates, where a fast activation step and a slower deactivation step are both needed. In other words, the choice of oxidizing agents and reductive agents is the key for the dissipative self-assembly of the ferrocenyl surfactant. Strategies to achieve redox control include adding chemically oxidizing agents such as H_2O_2, $K_2Cr_2O_7$, and $NaClO_4$.[11] Of these systems, the oxidizing process is fast and highly effective, which might not be suitable for constructing temporal redox assemblies which contain a fast reduction process (fast activation) and a slow oxidizing process (slow deactivation). Elegant strategies to fabricate the temporal artificial systems have utilized energy including enzyme-coupled programmed reactions,[12] which could bring inspiration for forming transient redox assemblies. It is reported that the temporal polymeric hydrogels achieved programmable gel dissociation by a D-glucose/glucose oxidase (GOX) enzymatic reaction, which ensures well-controlled acid generation.[13] Different from D-glucose, the GOX-catalyzed oxidation of β-D-glucose to gluconolactone and the concomitant reduction of molecular oxygen to H_2O_2 is a powerful tool to construct temporal supramolecular polymerization.[12] Inspired by this, the ferrocenyl surfactant can also be adjusted by GOX-catalyzed oxidation (slow deactivation) combined with a fast reducing process (fast activation), leading to a time-programmable aggregate transition.

GOX could provide a slow oxidation process; however, the dissipative self-assembly of the ferrocenyl surfactant in a complex system should also consider other circumstances such as a fast oxidation process (fast activation), temperature, and pH. Considering the different activation/deactivation processes through designing fuel input/energy dissipation, the redox-responsive surfactants undergoing an enzyme-catalyzed process is required, which is because the dissipative self-assembly could be adjusted by different kinds of enzymes that could tune the assembly and disassembly rate. For nanozymes,[14−17] many nanomaterials possessing excellent enzyme-like activities have been demonstrated, including noble-metal nanoparticles (NPs) and coordination polymers (CPs).[18−22] In particular, the application of CPs in enzyme mimicry has attracted great attention in recent years due to their abundant surfaces and channels and the presence of metal nodes providing possible catalytic active sites.[23−27] For example, Zhang's group achieved ultrasensitive detection of glucose by loading Pt NPs onto Fe-CPs to construct a hybrid nanozyme with high peroxidase-like properties.[28] Lin's group investigated the feasibility of modulating the catalytic efficiency of artificial nanozymes by disrupting the equilibrium state of CPs and distorting the lattice.[29] Sun's group synthesized novel CPs with multiple enzyme-like activities.[30] Wang's group investigated Ce-BPyDC CPs with peroxidase and oxidase activities for colorimetric biosensing.[31] However, CPs materials applied as an oxidizing agent for ferrocenyl surfactants are still in their infancy; the previously reported redox agents mainly focused on the common oxidizing agents such as sodium perchlorate,[32] potassium dichromate,[33] sodium chlorate,[34] sodium iodate, O_2, and so on. We believe that the catalytic oxidation of ferrocenyl surfactants through CPs would play a vital role in constructing redox-responsive materials.

In this study, we not only investigated the redox of the (11-ferrocenylundecyl) trimethylammonium bromide (FTMBr) using traditional O_2, H_2O_2, ascorbic acid, and $Na_2S_2O_3$, but also studied enzymes including GOX and Fe-CPs (Figure 1A). Surprisingly, Fe-CPs process high enzyme activities for the

https://doi.org/10.1021/acsomega.4c01715
ACS Omega 2024, 9, 23772−23781

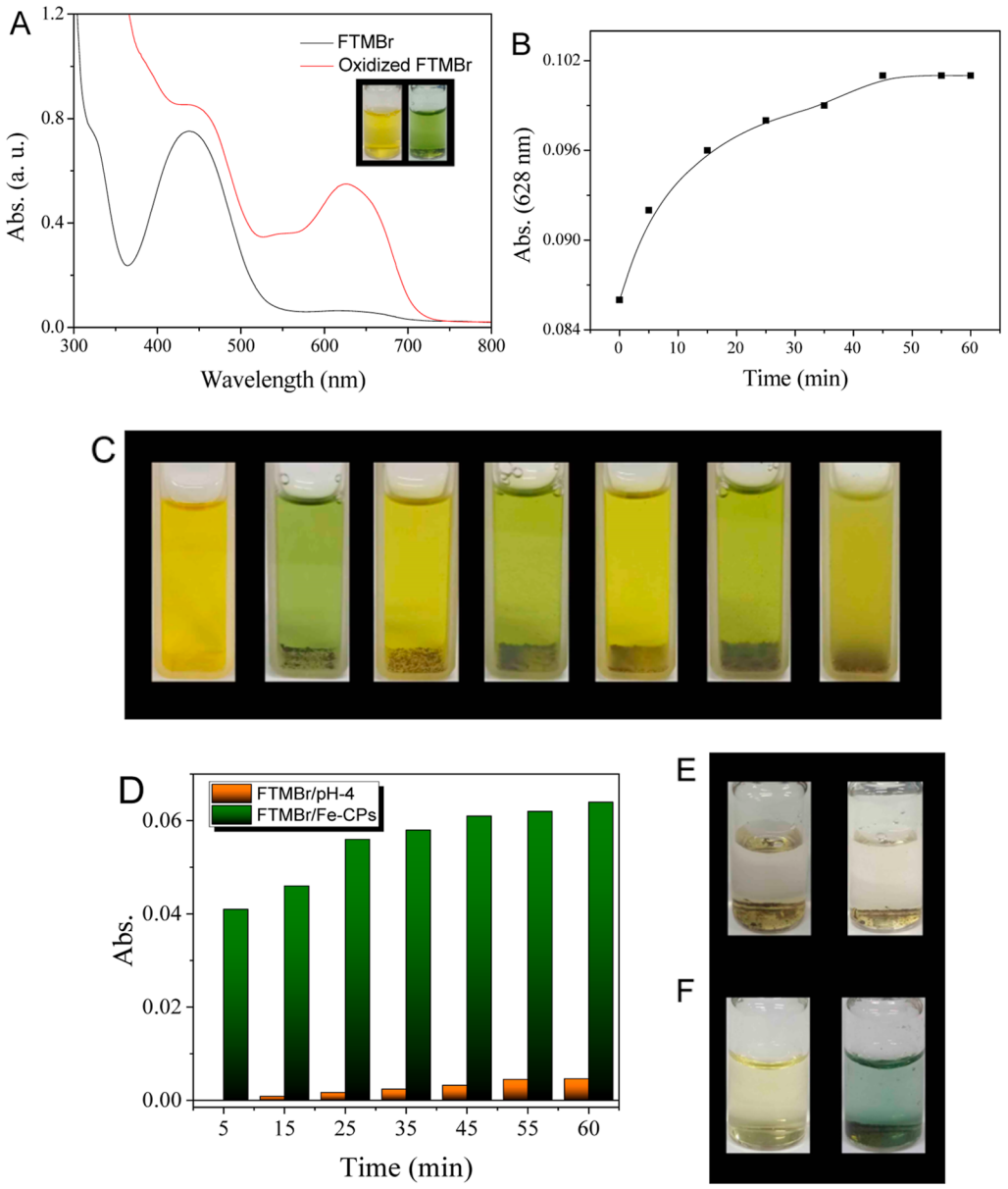

Figure 2. (A) UV absorption spectra and the corresponding photographs of FTMBr and ox-FTMBr with Fe-CPs-catalyzed oxidation. (B) Time-dependent absorbance changes at 628 nm for FTMBr with Fe-CPs. (C) Pictures of FTMBr showing the redox cycles. (D) Time-dependent absorbance at 628 nm of FTMBr (pH-4) and FTMBr with Fe-CPs. (E) Photographs of Fe-CPs aqueous solution at different times [0 min, (left) and 6 min (right)]. (F) Photographs of FTMBr with Fe-CPs (right) or without Fe-CPs (left; incubation time, 6 min).

FTMBr oxidizing process. Moreover, Fe-CPs, as an oxidase-like enzyme, exhibits a promising catalytic activity in the pH range from 3 to 9 and the oxidase-like activity of Fe-CPs is also resistant to temperature, demonstrating that Fe-CPs have good stability. It is particularly important for the catalyst to maintain stability under different reaction conditions, because the integrity of the structure will greatly affect the catalytic activity of the catalyst.[35] Enzyme-coupled programmed reactions are an elegant strategy to construct temporal systems. Investigating the catalytic conditions and rates is a subject worth studying for temporal ferrocenyl assemblies. However, it is regrettable that the catalytic rate of Fe-CPs is not satisfied with the slow deactivation in dissipative self-assembly and Fe-CPs can still not replace the role of GOX. Even so, we believe the catalytic oxidation of the ferrocenyl surfactants through CPs will play a vital role in constructing redox-responsive materials. Eventually, we choose another enzyme of GOX to fabricate a GOX-catalyzed, glucose-fueled transient transition between hydrophobic FTMBr and hydrophilic oxidizing FTMBr (ox-FTMBr), combined with a faster-reducing agent of $Na_2S_2O_3$. The micelles of the ferrocenyl surfactant with positive charges can serve as a tool to capture DNA molecules.[36] Once FTMBr was oxidized by glucose/GOX, leading to a hydrophilic enhancement for the surfactant, and a disassembly process of the FTMBr micelle into single ox-FTMBr was observed. Thus, glucose-fueled dissipative self-assembly of FTMBr could work as an efficient tool to realize a time-programmable capture and release of DNA (Figure 1B).

2. RESULT AND DISCUSSION

2.1. Cationic "Redox-Switchable" Ferrocenyl Surfactants of FTMBr. It is reported that a ferrocene salt was made

https://doi.org/10.1021/acsomega.4c01715
ACS Omega 2024, 9, 23772−23781

Scheme 1. Schematic Illustration of Glucose-Fueled Transient Cycle of FTMBr and Ox-FTMBr by $Na_2S_2O_3$ and Glucose Oxidase (GOX) in the Presence of O_2[a]

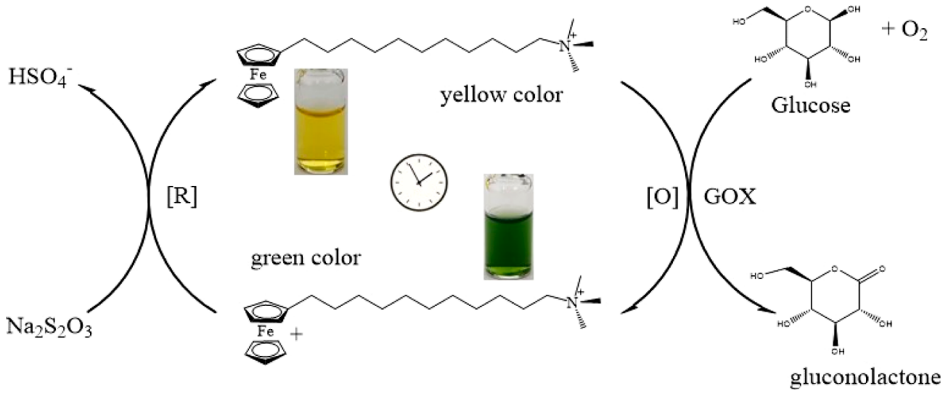

[a][R] = reduction, [O] = oxidation. Images of vials reveal the colors of oxidation state and reduction state.

by the acid−base reaction of fatty acid and dimethylaminomethyl ferrocene, accompanied by the formation of a self-supporting gel. An oxidizing $Fe(ClO_4)_3$ helped in the dissipation of energy by converting dimethylaminomethyl ferrocene to oxidized waste and the gel transferred to sol.[37] Considering the different activation/deactivation processes through designing fuel input/energy dissipation in dissipative self-assembly, we synthesized the FTMBr, which has a better reversible regulation of the charge and hydrophobicity containing ferrocenyl groups, leading to a transition of the self-assembled structure. As shown in Figure S1B in the Supporting Information, the redox-responsive FTMBr was prepared as previously described through the four-step procedure.[38] The ^1H NMR result proved the successful synthesis of FTMBr (Figure S1C). The mass spectra of FTMBr (Figure S1D) also confirmed this result. As shown in Figure S1A, the electron gain and loss of FTMBr lay the foundation for redox reactions.[39−45] This switchable process can be realized by redox stimuli as oxidizing/reducing agents or electrochemical methods. The method of carrying out simple and convenient catalytic oxidation of ferrocene plays an important role in the development of the redox properties of ferrocene. Figure S2A shows that the ox-FTMBr has a green color with a 628 nm UV characteristic absorption peak, while reductive FTMBr is yellow with an absorption peak at 437 nm in the presence of ascorbic acid. To test the oxidation capacity of H_2O_2, the effects of pH, temperature, H_2O_2 concentrations, and time were investigated (Figure S3A−D), and the optimal reaction conditions were pH-6, room temperature, 2 M, and 10 min. Besides, the reducing capacity of ascorbic acid was evaluated at varying ascorbic acid concentrations and temperatures (Figures S4 and S5) and the optimal reaction conditions were 0.3 g and room temperature. As shown in Figure S6, the higher the concentration of H_2O_2, the faster the oxidation rate of FTMBr with a higher absorbance at 628 nm. What's more, the absorbance of ox-FTMBr at 628 nm gradually decreased with ascorbic acid (Figure S2B), indicates that ox-FTMBr was successfully reduced to FTMBr.

2.2. Fe-CPs Served as a Novel Oxidase-like Enzyme for FTMBr Oxidation. The Fe-CPs were synthesized via a one-pot hydrothermal method. Furthermore, as shown in Figure S7C, FT-IR analysis was applied to prove the successful fabrication of Fe-CPs. Clearly, the characteristic peak at 1220 cm^{-1} represented the stretch vibration of C−N, and the characteristic peak at 1652 cm^{-1} indicated the bond of C═N. Compared with organic linkers, the peak of C═N significantly shifted to lower frequency in the spectra, indicating the involvement of azomethine nitrogen in the chelation to Fe ions.[46] Fe-CPs have the catalytic activities of glucose-like oxidases and oxidases by using a chromogenic substrate (Figure S7A,B); therefore, Fe-CPs were added into the FTMBr system to investigate the oxidation ability of Fe-CPs. As shown in Figure 2A, a strong absorption peak at 628 nm can be observed, indicating the presence of ox-FTMBr by oxidation catalyzed from Fe-CPs. It is evident from Figure 2A that the sample solution changes from yellow to green when ox-FTMBr appears. Figure 2B shows the UV−vis spectra of FTMBr at 628 nm recorded from 0, 5, 15, 25, 35, 45, 55, and 60 min, indicating that Fe-CPs have oxidase-like activity. Inspired by the reversible oxidation−reduction properties of FTMBr, we found that a cyclic transition from FTMBr to ox-FTMBr can be achieved by the circular addition of Fe-CPs and (Figures 2C and S8). As shown in Figure S9A, there were no significant absorbance changes can be observed from pH 3 to 9; in other words, the high catalytic activity of Fe-CPs was almost unaffected by pH. Figure S9B indicates that Fe-CPs also had high oxidase-like activity in the range of 20−60 °C. These results further demonstrate the excellent properties of Fe-CPs as oxidase-like enzymes.

FTMBr can be readily oxidized to blue paramagnetic ferrocenium in acidic solutions. Furthermore, the iron ions could be affected under various acid−base conditions, which may disturb the color changes of the FTMBr solution. Therefore, the effect of the pH on Fe-CPs/FTMBr catalytic systems is further discussed. Before adding Fe-CPs, the pH of the FTMBr solution was 6.6, but it changed to pH 3.62 after Fe-CPs addition. To exclude the production of ox-FTMBr in the acidic condition, the FTMBr solution was tuned to pH below 4; subsequently, the UV spectrum was recorded with different times (Figure S10). As shown in Figures 2D and S10A−C, when the FTMBr solution is at pH 3.44, the FTMBr solution still showed a yellow color and the reduction peak at 437 nm, indicating that FTMBr still remains in a reduction state. Furthermore, in the presence of Fe-CPs, the absorption peak intensity at 628 nm can be monitored and these phenomena further verified that the oxidation of FTMBr was independent of the acidic condition. In addition, the thermal and chemical stability of CPs is a vital factor in determining its

https://doi.org/10.1021/acsomega.4c01715
ACS Omega 2024, 9, 23772−23781

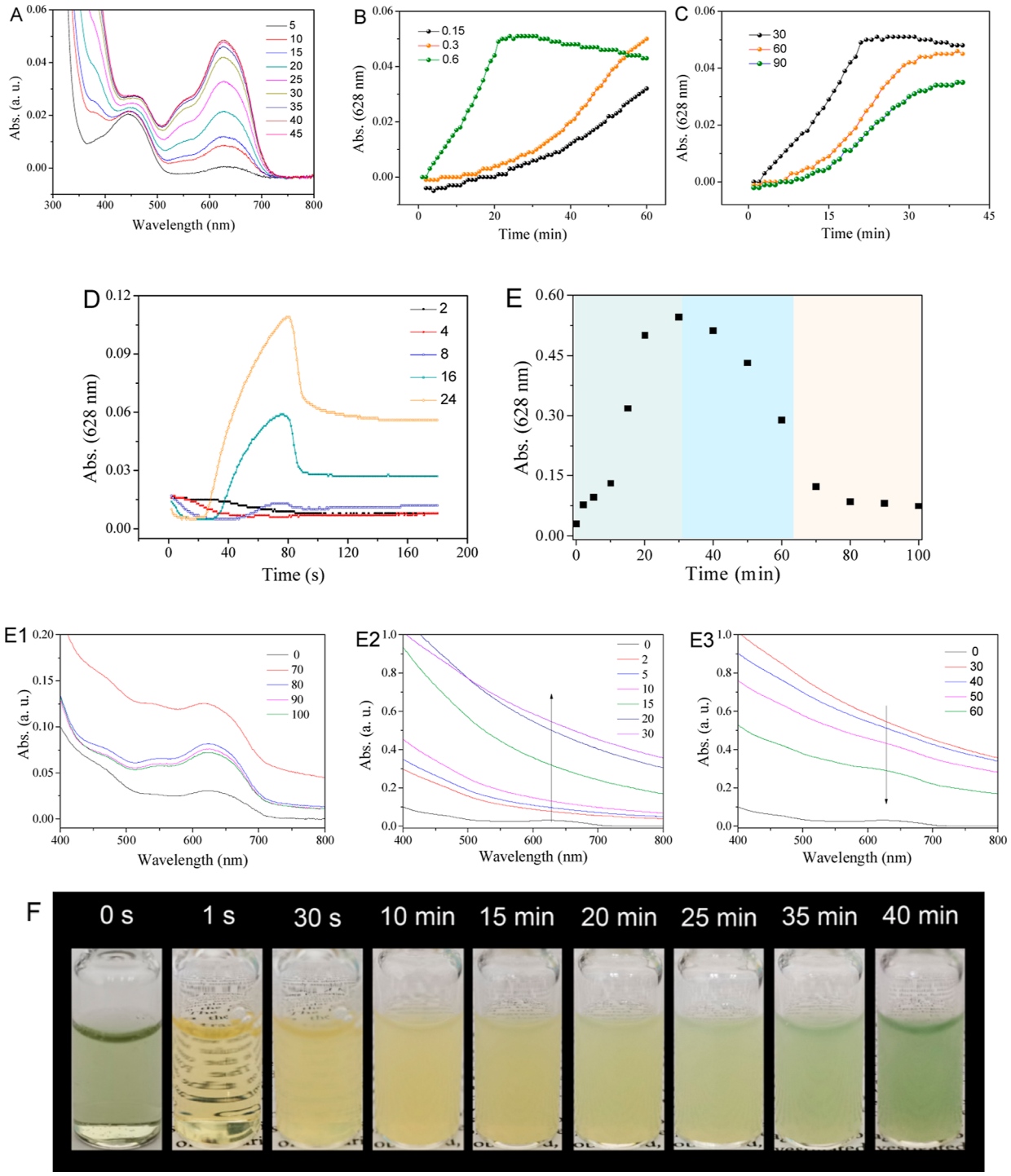

Figure 3. (A) UV spectra of FTMBr oxidized by GOX at different times (min). (B) Dependence of the absorbance changes at 628 nm on increasing time with different GOX concentrations (0.15, 0.3, and 0.6 g/L). Reaction conditions: glucose (30 mM). (C) Time-dependent absorbance changes at 628 nm with different glucose concentrations (30, 60, and 90 mM). Reaction conditions: GOX (0.6 g/L). (D) Time-dependent absorbance changes at 628 nm using different concentrations of $Na_2S_2O_3$ (2, 4, 8, 16, and 24 mM). (E) Time-dependent absorbance changes at 628 nm of GOX-catalyzed, glucose-fueled cycle of nonequilibrium FTMBr and ox-FTMBr. The UV−vis spectra of the nonequilibrium FTMBr and ox-FTMBr in the range of 70−100 (E1), 0−30 (E2), and 30−60 min (E3). (F) Photographs of the nonequilibrium FTMBr and ox-FTMBr. All the samples include FTMBr (2 mM); GOX (0.21 g/L); glucose (90 mM); and $Na_2S_2O_3$ (6 mM).

structural integrity, which ultimately leads to its properties being affected. Furthermore, photographs of Fe-CPs in ultrapure water at different times were taken to investigate the stability of Fe-CPs in aqueous solution. As shown in Figure 2E, no significant changes were observed after 6 min, suggesting that the green solution was not due to Fe-CPs. By contrast, Fe-CPs were added to the FTMBr solution and incubated for 6 min (Figure 2F). Obvious green color can be observed indicating the generation of ox-FTMBr from catalytic oxidation rather than the effect of Fe-CPs, indicating the high oxidase-like catalytic activity of Fe-CPs.

https://doi.org/10.1021/acsomega.4c01715
ACS Omega 2024, 9, 23772−23781

2.3. Transient FTMBr Mediated by Redox Regulation. Since ferrocene is known to acutely respond to changes in the redox environment, to achieve the transient formation of compartments, the challenge is to find a subtle balance of reduction−oxidation rates.[37] Fe-CPs synthesized in this work are oxidase-like enzymes that could exhibit a promising catalytic oxidation of the FTMBr . As shown in Figure S11, the catalytic oxidation rates of CPs are much higher than that of GOX. Obviously, this result leads to a conclusion that Fe-CPs are not suitable in temporal ferrocenyl assemblies, and Fe-CPs can still not replace the role of GOX. The faster oxidation in the presence of Fe-CPs is not satisfied with a slow oxidation step in an energy dissipation process. Interestingly, the enzymatic coupling provides multiple cues, including the concentrations of glucose oxidase and glucose, which can be modulated to control the kinetics of oxidation appropriately. As shown in Scheme 1, for the fast reduction step, a strong reducing agent of $Na_2S_2O_3$ was used as chemical fuel (activator) to achieve the transition of ox-FTMBr to FTMBr. For the slow oxidation step, we used an enzymatic oxidation pathway by GOX as a delayed deactivator. Glucose, which was a reaction substrate of GOX, along with oxygen was catalyzed by GOX; it then generated a strong oxidizing agent, hydrogen peroxide.[12] We recorded the conversion rate of FTMBr to ox-FTMBr by recording the absorbance at 628 nm by using a UV−vis spectrometer. A gradual increase in the absorbance of 628 nm was observed with an increasing GOX (Figure S12A−C).

The time effected on the catalyzed oxidation of FTMBr with GOX also was investigated. Figure 3A displays that the oxidation peak of FTMBr at 628 nm was gradually enhanced with time. As shown in Figure 3B,C, the higher concentration of GOX or glucose leads to a higher absorbance intensity at 628 nm as well as a faster oxidation rate for the FTMBr, which indicates that the amount of ox-FTMBr gradually increases with time. Furthermore, a yellow coloration appeared with a new absorption at 437 nm in the presence of corresponding to the production of FTMBr. As expected, the absorbance at 628 nm of ox-FTMBr decreased rapidly at a low concentration of $Na_2S_2O_3$, as shown in Figure 3D. However, with a higher concentration of of 8−24 mM, the absorbance at 628 nm showed a sharp rise, accompanied by obvious turbidity of solution (Figure 3D). The oxidation of ferrocene to ferrocenium results in an enhanced hydrophilicity for FTMBr. In contrast, the reduction and lost electron of ferrocenium to ferrocene results in a hydrophobicity change for FTMBr.[11] This is the fundamental reason for the turbidity of the reducing FTMBr solution as well as a higher absorbance in its UV−vis spectra. By observing the absorption spectra of the reaction between various $Na_2S_2O_3$ and ox-FTMBr, we can intuitively understand the conversion from ox-FTMBr to FTMBr, that is, the absorbance intensity of the oxidation peak is weakened, and the absorbance intensity of the reduction peak is enhanced (Figure S13).

To construct a transient redox FTMBr, a faster reducing agent of and a slower GOX catalyzed, the glucose-fueled process is needed in dissipative self-assembly. As shown in Figure 3E, the ox-FTMBr was mixed with , GOX, and the time-dependent absorption changes at 628 nm of ox-FTMBr were monitored by using a UV−vis spectrometer. First, due to the faster reduction of the reduction of ox-FTMBr into FTMBr was depicted by the decrease in absorbance at 628 nm. As shown in Figure 3E (green region) and E3, upon addition of , the UV−vis baseline of ox-FTMBr sharply increased within 30 min and reached a maximum absorbance at 750 nm (Figure S14), while the absorbance peak at 628 nm disappeared during this time. The rapidly turbid solution results from an increasing hydrophobicity for ferrocene. This result is in accord with the production of transient FTMBr after adding in Figure 3D. Then, the UV−vis baseline continued to decrease within 30−60 min. as shown in Figure 3E (blue region) and E3 and Figure S14. This is owing to the catalytic oxidation of glucose by GOX playing a predominance, and the transient FTMBr returned to ox-FTMBr. With time, the turbidity of solution greatly reduced (Figure S14); especially, the absorbance peak at 628 nm weakened gradually, as shown in Figure 3E (yellow region) and E1, due to the decreased turbidity. The variation tendency is a dynamic balance of fast reduction (activation) and slow oxidation (deactivation), accompanying complex optical changes including turbidity and color. We make attempts to visualize the transient cycle, as shown in Figure 3F and 3E, before the addition of glucose, GOX, and $Na_2S_2O_3$, a clear green solution with an absorption intensity at 628 nm can be observed. In the redox cycle processes, the oxidation of FTMBr relies on the concentrations of glucose and GOX, and the reduction rate becomes extremely high when the concentration of is high. As shown in Figure 3F, we can observe that the color of the original ox-FTMBr solution autonomously changed from clear green (0 s) to clear yellow (1 s) and to turbid yellow (within 30 min) gradually; subsequently, it retransferred into turbid green at 35 min. The FTMBr went through the oxidation state to the reduction state and then to the oxidation state, and the whole redox lifetime was about 100 min, as shown in Figure 3E. Importantly, the lifetime is time-controlled by the competing rates of $Na_2S_2O_3$ reduction and GOX catalytic oxidation.

2.4. DNA is Captured and Released by Redox-Dissipative FTMBr. The fast reduction and slow GOX catalytic oxidation bring about an automatic redox switch accompanying the optical change for FTMBr. More importantly, this coupling solution set a controllable lifetime for a transition between the hydrophilic ferrocenium and hydrophobic ferrocene in the surfactant. For reducing FTMBr, the hydrophobicity interaction coming from ferrocenyl tail chain could bond single surfactant into micelles with a critical micelle concentration of 0.1 mM.[47] The FTMBr micelles with positive charges can serve as a tool to capture DNA molecules.[36] The electrostatic interactions are the main driving force for DNA/surfactant self-assemblies; the hydrophobic interaction of surfactants has a synergistic effect on the self-assembly process.[48] Therefore, the factors affecting the electrostatic and hydrophobic interactions can regulate the self-assembly process of DNA and surfactant. However, once FTMBr was catalytically oxidized by glucose/GOX, FTMBr gains one electron, leading to a hydrophilic enhancement for the surfactant. At this time, there will occur a disassembly process of FTMBr micelle into single ox-FTMBr. It is reported that the molecules that can catch or condense DNA should possess at least 3 positive charges.[49] However, the single ox-FTMBr has 2 positive charges, which is not enough to catch DNA molecules. Inspired by this, glucose-fueled dissipative self-assembly of FTMBr could work as an efficient tool to realize the time-programmable capture and release of DNA.

The change in the charge ratio of the surfactant and DNA has an important effect on the electrostatic interaction between them. The phase separation region usually appears in the phase

https://doi.org/10.1021/acsomega.4c01715
ACS Omega 2024, 9, 23772−23781

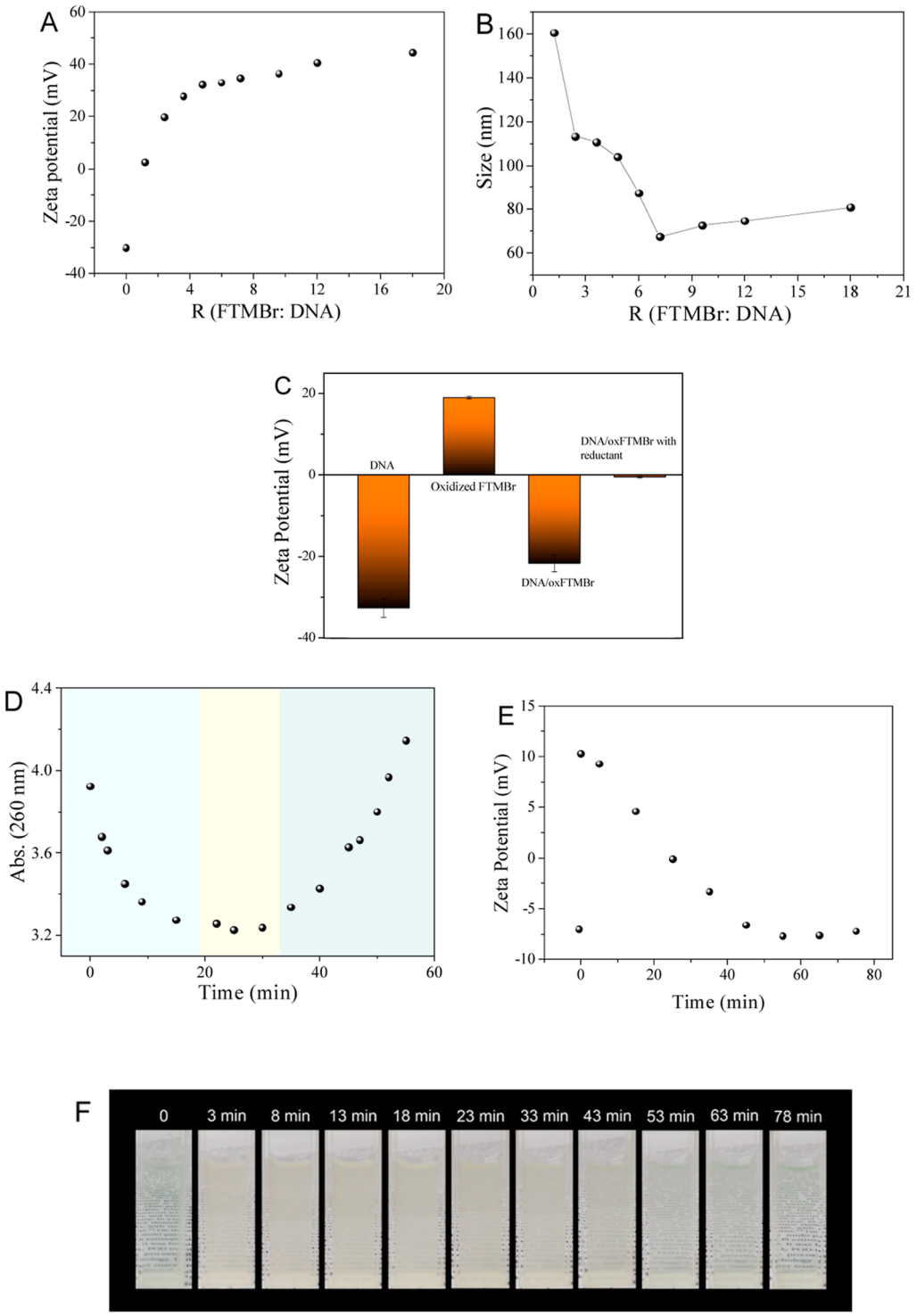

Figure 4. (A) Zeta potential. (B) Particle size of DNA/FTMBr complexes at different *R* (molar ratio of FTMBr: DNA), *R* is 1.2, 2.4, 3.6, 4.8, 6, 7.2, 9.6, 12, and 18. (C) Zeta potential of DNA, FTMBr/DNA complexes, ox-FTMBr/DNA solution, and ox-FTMBr/DNA with $Na_2S_2O_3$ solution. (D) Time-dependent absorbance intensity at 260 nm of temporal FTMBr/DNA complexes in a GOX-catalyzed, glucose-fueled dissipative self-assembly. Reaction condition in (D) includes 30 mM glucose; 0.2 g/L GOX; and 2.4 mM. (E) Time-dependent zeta potential of transient FTMBr/DNA complexes. (F) Images demonstrating color and turbidity changes in the redox-transient FTMBr/DNA complexes.

diagram with a change of DNA or surfactant concentration. When negatively charged DNA molecules are electrostatically self-assembled with the FTMBr, the zeta potential of the DNA/FTMBr mixture is gradually increased. As shown in Figure 4A, the zeta potential value of DNA is −30.1 mV, and the zeta potential of the DNA/FTMBr complex gradually increased to 44.4 mV with an increase of *R* (*R* is the molar ratio of FTMBr and DNA). When *R* = 1.2, the zeta potential is close to 0 and a large amount of precipitation is produced at this isoelectric point. This is because the introduction of the FTMBr significantly shields the electrostatic repulsion between negatively charged DNA and reduces the stability of the DNA/

https://doi.org/10.1021/acsomega.4c01715
ACS Omega 2024, 9, 23772−23781

FTMBr complex, leading to the occurrence of aggregation behavior. The zeta potential provides indications on stability of colloid particles; usually, ±0−10, ±10−20, ±20−30, and ≥30 mV are regarded as highly unstable, relatively stable, moderately stable, and highly stable, respectively. According to the DLVO theory, colloid stability depends on the sum of van der Waals attractive forces and electrostatic repulsive forces due to the electric double layer.[50] The negatively charged DNA has a good water solubility; however, with an increasing R of the FTMBr, the production of FTMBr/DNA complexes comes from the electrostatic interaction of surfactant and DNA, showing a gradually increased zeta potential. Once R reaches 1.2, the zeta potential becomes 0 mV, which indicates that the complexes are highly unstable, leading to producing precipitation. At this isoelectric point, as shown in Figures S15 and 4B, their sizes are the largest, and the DNA/FTMBr is unstable and easy to form precipitates. When R > 2.4, the DNA-FTMBr complex precipitation gradually decreased due to the high positivity of the zeta potential value. The size of DNA complexes decreased from about 160 to 65 nm and then increased to 80 nm, as shown in Figure 4B, which is different from FTMBr of 65.6 nm shown in Figure S16.

By controlling the redox state of the FTMBr group, the charge and hydrophilicity of the FTMBr can be adjusted, resulting in a transition of the self-assembled structure.[11] By adding oxidants or reducing agents to the DNA/FTMBr complex solution, the redox response of FTMBr groups can induce the color-indicated self-assembled structural transformation of DNA/FTMBr complexes. As shown in Figure 4C, we demonstrated the feasibility of the redox dissipation interaction between FTMBr and DNA using zeta potential values, which were negative for DNA and positive for the FTMBr. When the ox-FTMBr was mixed with DNA, the zeta potential of the mixed solution was still negative, indicating that the ox-FTMBr cannot interact with DNA. Subsequently, the reducing agent of $Na_2S_2O_3$ was added to the mixture of the ox-FTMBr and DNA. As expected, the mixture was immediately turbid, which was around the isoelectric point of DNA. At this time, the ox-FTMBr is rapidly reduced by the reducing agent , and then the FTMBr interacts with DNA to form aggregates. Figure 4E shows the time-dependent zeta potential of the DNA/FTMBr containing GOX. The zeta potential showed a sharp increment at 0 s owing to the ox-FTMBr and decreased during the first 20 min, indicating that DNA was captured by the FTMBr after reduction. Subsequently, GOX gradually induced a slow oxidation process with ox-FTMBr generation. Therefore, DNA was gradually released, accompanied by the zeta potential slowly moving toward negative values. Subsequently, we characterized the redox dissipative self-assembly of FTMBr and DNA by monitoring the absorbance at 260 nm. The characteristic peak of DNA at 260 nm can represent the process of DNA being captured and released. As shown in Figure 4D, first, ox-FTMBr could be reduced by sodium thiosulfate. The reduced FTMBr behaved as positively charged aggregates to bind with DNA, resulting in a rapid decrease in absorbance at 260 nm. With time, GOX gradually played a leading role in generating ox-FTMBr, which cannot interact with the DNA, resulting in a gradual release of DNA, showing an increment of absorbance intensity at 260 nm. We took photographs of the redox dissipation process in order to understand the process of redox dissipation between FTMBr and DNA. As shown in Figure 4F, when the time was 0 s, the mixed solution was composed of the oxidized FTMBr and DNA. Meanwhile, the mixture showed a light blue-green color and no obvious Tyndall phenomenon, suggesting that there were no aggregates of FTMBr-DNA. Once the dissipation was activated by the oxidized FTMBr was reduced to FTMBr which spontaneously interacted with DNA to produce aggregates. As time progressed, more ox-FTMBr were generated, ascribed to the predominance of GOX catalytic oxidation, which allowed for a DNA release to occur spontaneously. The mixed solution that showed yellow turbidity gradually disappeared and the light yellow gradually changed to clear blue-green. These results confirm the successful application of a time-controlled and spontaneous capture and release of DNA by FTMBr.

3. CONCLUSIONS

In this work, we synthesized a redox-responsive surfactant of FTMBr. The obtained Fe-CPs materials can serve as a highly effective oxidase-like enzyme to induce the oxidation of FTMBr. Fe-CPs have high oxidase-like activities over a wide range of temperatures and pH. The ferrocenyl surfactant undergoes CPs catalysis which brings more choice for the activation/deactivation process through designing fuel input/energy dissipation in dissipative self-assembly; meanwhile, this also builds a bridge between the CPs materials and surfactants. In addition, different GOX-catalyzed, glucose-fueled transient FTMBr assemblies have been fabricated. In the redox dissipation process, $Na_2S_2O_3$ was used as a reducing agent, and the oxidation of FTMBr was generated by GOX. The temporal FTMBr assemblies are highly positively charged due to the hydrophobic interaction of FTMBr, leading to a time-controlled and autonomous DNA capture and release process. The intelligent use of enzymes including CPs and GOX in ferrocene-based surfactants will pave the way to construct stable or transient ferrocenyl self-assemblies.

■ ASSOCIATED CONTENT

Supporting Information

The Supporting Information is available free of charge at https://pubs.acs.org/doi/10.1021/acsomega.4c01715.

Chemical and materials, characterization, the synthesis of FTMBr and Fe-CPs, redox properties of FTMBr, Fe-CPs as an oxidase-like enzyme, redox dissipation of FTMBr, the capture and release of DNA, schematic diagram, synthesis, ^{1}H NMR, and mass spectrum of the FTMBr; photographs and UV of FTMBr using H_2O_2 or ascorbic acid; UV spectra of FTMBr with H_2O_2 at different concentrations, pH, temperatures, and times; UV spectra of ox-FTMBr with ascorbic acid; UV spectra of ox-FTMBr with ascorbic acid at different temperatures; UV spectra of FTMBr with H_2O_2; UV spectra and photographs of Fe-CPs as glucose-like oxidase, FT-IR spectrum of Fe-CPs and organic linker; UV spectra showing the redox cycles of FTMBr; effect of pH and temperature on the peroxidase activity of Fe-CPs; absorbance of FTMBr at pH 4 at different times, UV spectrum and photograph of FTMBr at pH 3.44; time-dependent absorbance at 628 nm of FTMBr with GOX and with Fe-CPs; UV spectra of ox-FTMBr at different times; and UV spectra of ox-FTMBr with (PDF)

https://doi.org/10.1021/acsomega.4c01715
ACS Omega 2024, 9, 23772−23781

AUTHOR INFORMATION

Corresponding Authors

Ling Wang − *School of Chemistry and Chemical Engineering, Center of Cosmetics, Qilu Normal University, Jinan 250200 Shandong Province, China*; orcid.org/0009-0003-2111-5202; Email: wangling0824@qlnu.edu.cn

Yawen Li − *School of Chemistry and Chemical Engineering, Center of Cosmetics, Qilu Normal University, Jinan 250200 Shandong Province, China*; Email: sgliyawen@163.com

Authors

Ting Liu − *School of Chemistry and Chemical Engineering, Center of Cosmetics, Qilu Normal University, Jinan 250200 Shandong Province, China*

Liwei Zhu − *School of Chemistry and Chemical Engineering, Center of Cosmetics, Qilu Normal University, Jinan 250200 Shandong Province, China*

Chencan Li − *School of Chemistry and Chemical Engineering, Center of Cosmetics, Qilu Normal University, Jinan 250200 Shandong Province, China*

Yang Yu − *School of Chemistry and Chemical Engineering, Center of Cosmetics, Qilu Normal University, Jinan 250200 Shandong Province, China*

Zhuo Zhang − *School of Chemistry and Chemical Engineering, Center of Cosmetics, Qilu Normal University, Jinan 250200 Shandong Province, China*

Huizhong Liu − *School of Mechatronics and Automobile Engineering, Yantai University, Yantai 264005 Shandong Province, China*

Complete contact information is available at: https://pubs.acs.org/10.1021/acsomega.4c01715

Notes

The authors declare no competing financial interest.

ACKNOWLEDGMENTS

This work was financially supported by the National Nature Science Foundation, China. (no. 21902090, 22202112) and by the Shandong Provincial Youth Innovation Team Development Plan (no. 2021KJ096) and by the Youth Project of Natural Science Foundation of Shandong Province (no. ZR2022QB037, ZR2022QB208).

REFERENCES

(1) Dai, K.; Fores, J. R.; Wanzke, C.; Winkeljann, B.; Bergmann, A. M.; Lieleg, O.; Boekhoven, J. Regulating Chemically Fueled Peptide Assemblies by Molecular Design. *J. Am. Chem. Soc.* **2020**, *142*, 14142−14149.

(2) Deng, J.; Liu, W.; Sun, M.; Walther, A. Dissipative Organization of DNA Oligomers for Transient Catalytic Function. *Angew. Chem., Int. Ed.* **2022**, *61*, No. e202113477.

(3) Grötsch, R. K.; Wanzke, C.; Speckbacher, M.; Angi, A.; Rieger, B.; Boekhoven, J. Pathway Dependence in the Fuel-Driven Dissipative Self-Assembly of Nanoparticles. *J. Am. Chem. Soc.* **2019**, *141*, 9872−9878.

(4) Wang, G.; Sun, J.; An, L.; Liu, S. Fuel-Driven Dissipative Self-Assembly of a Supra-Amphiphile in Batch Reactor. *Biomacromolecules* **2018**, *19*, 2542−2548.

(5) Colomer, I.; Morrow, S. M.; Fletcher, S. P. A transient self-assembling self-replicator. *Nat. Commun.* **2018**, *9*, 2239−2244.

(6) Cardona, M. A.; Chen, R.; Maiti, S.; Fortunati, I.; Ferrante, C.; Gabrielli, L.; Das, K.; Prins, L. J. Time-Gated Fluorescence Signalling under Dissipative Conditions. *Chem. Commun.* **2020**, *56*, 13979−13982.

(7) Seoane, A.; Brea, R. J.; Fuertes, A.; Podolsky, K. A.; Devaraj, N. K. Biomimetic Generation and Remodeling of Phospholipid Membranes by Dynamic Imine Chemistry. *J. Am. Chem. Soc.* **2018**, *140*, 8388−8391.

(8) Estrada-Osorio, D. V.; Escalona-Villalpando, R. A.; Gutiérrez, A.; Arriaga, L. G.; Ledesma-García, J. Poly-L-lysine-Modified with Ferrocene to Obtain a Redox Polymer for Mediated Glucose Biosensor Application. *Bioelectrochemistry* **2022**, *146*, 108147−108154.

(9) Roy, G.; Gupta, R.; Ranjan Sahoo, S. R.; Saha, S.; Asthana, D.; Chandra Mondal, P. Ferrocene as an Iconic Redox Marker: from Solution Chemistry to Molecular Electronic Devices. *Coord. Chem. Rev.* **2022**, *473*, 214816−214838.

(10) Moreno, S.; Hübner, H.; Effenberg, C.; Boye, S.; Ramuglia, A.; Schmitt, D.; Voit, B.; Weidinger, I. M.; Gallei, M.; Appelhans, D. Redox- and pH-Responsive Polymersomes with Ferrocene Moieties Exhibiting Peroxidase-like, Chemoenzymatic Activity and H_2O_2-Responsive Release Behavior. *Biomacromolecules* **2022**, *23*, 4655−4667.

(11) Zhao, W.; Hao, J. Colloidal Chirality in Wormlike Micellar Systems Exclusively Originated from Achiral Species: Role of Secondary Assembly and Stimulus Responsivity. *J. Colloid Interface Sci.* **2016**, *478*, 303−310.

(12) Spitzer, D.; Rodrigues, L. L.; Straßburger, D.; Mezger, M.; Besenius, P. Tuneable Transient Thermogels Mediated by a pH- and Redox-Regulated Supramolecular Polymerization. *Angew. Chem., Int. Ed.* **2017**, *56*, 15461−15465.

(13) Hu, K.; Sheiko, S. S. Time Programmable Hydrogels: Regulating the Onset Time of Network Dissociation by a Reaction Relay. *Chem. Commun.* **2018**, *54*, 5899−5902.

(14) Huang, Y.; Ren, J.; Qu, X. Nanozymes: Classification, Catalytic Mechanisms, Activity Regulation, and Applications. *Chem. Rev.* **2019**, *119*, 4357−4412.

(15) Liang, M.; Yan, X. Nanozymes: From New Concepts, Mechanisms, and Standards to Applications. *Acc. Chem. Res.* **2019**, *52*, 2190−2200.

(16) Wei, H.; Wang, E. Nanomaterials with Enzyme-like Characteristics (Nanozymes): Next-Generation Artificial Enzymes. *Chem. Soc. Rev.* **2013**, *42*, 6060−6093.

(17) Barber, J. Photosynthetic Energy Conversion: Natural and Artificial. *Chem. Soc. Rev.* **2009**, *38*, 185−196.

(18) Li, S.; Zhao, X.; Yu, X.; Wan, Y.; Yin, M.; Zhang, W.; Cao, B.; Wang, H. Fe_3O_4 Nanozymes with Aptamer-Tuned Catalysis for Selective Colorimetric Analysis of ATP in Blood. *Anal. Chem.* **2019**, *91*, 14737−14742.

(19) Demkiv, O.; Stasyuk, N.; Serkiz, R.; Gayda, G.; Nisnevitch, M.; Gonchar, M. Peroxidase-Like Metal-Based Nanozymes: Synthesis, Catalytic Properties, and Analytical Application. *Appl. Sci.* **2021**, *11*, 777−790.

(20) Wang, G.; Zhang, J.; He, X.; Zhang, Z.; Zhao, Y. Ceria Nanoparticles as Enzyme Mimetics. *Chin. J. Chem.* **2017**, *35*, 791−800.

(21) Yin, M.; Li, S.; Wan, Y.; Feng, L.; Zhao, X.; Zhang, S.; Liu, S.; Cao, P.; Wang, H. A Selective Colorimetric Strategy for Probing Dopamine and Levodopa through the Mussel-Inspired Enhancement of Fe_3O_4 Catalysis. *Chem. Commun.* **2019**, *55*, 12008−12011.

(22) Zhao, X.; Li, S.; Yu, X.; Gang, R.; Wang, H. In Situ Growth of CeO_2 on g-C_3N_4 Nanosheets toward a Spherical g-C_3N_4/CeO_2 Nanozyme with Enhanced Peroxidase-Like Catalysis: a Selective Colorimetric Analysis Strategy for Mercury(II). *Nanoscale* **2020**, *12*, 21440−21446.

(23) Xu, W.; Jiao, L.; Yan, H.; Wu, Y.; Chen, L.; Gu, W.; Du, D.; Lin, Y.; Zhu, C. Glucose Oxidase-Integrated Metal-Organic Framework Hybrids as Biomimetic Cascade Nanozymes for Ultrasensitive Glucose Biosensing. *ACS Appl. Mater. Interfaces* **2019**, *11*, 22096−22101.

(24) Hu, Y.; Dai, L.; Liu, D.; Du, W.; Wang, Y. Progress & Prospect of Metal-Organic Frameworks (MOFs) for Enzyme Immobilization (Enzyme/MOFs). *Renew. Sust. Energy Rev.* **2018**, *91*, 793−801.

https://doi.org/10.1021/acsomega.4c01715
ACS Omega 2024, 9, 23772−23781

(25) Guo, J.; Yang, L.; Gao, Z.; Zhao, C.; Mei, Y.; Song, Y.-Y. Insight of MOF Environment-Dependent Enzyme Activity via MOFs-in-Nanochannels Configuration. *ACS Catal.* **2020**, *10*, 5949−5958.
(26) Silva, A. R. M.; Alexandre, J.; Souza, J. E. S.; Neto, J. G. L.; de Sousa Júnior, P.; Rocha, M. V. P.; dos Santos, J. The Chemistry and Applications of Metal-Organic Frameworks (MOFs) as Industrial Enzyme Immobilization Systems. *Molecules* **2022**, *27*, 4529−4556.
(27) Wang, Y.; Zhu, Y.; Binyam, A.; Liu, M.; Wu, Y.; Li, F. Discovering the Enzyme Mimetic Activity of Metal-Organic Framework (MOF) for Label-Free and Colorimetric Sensing of Biomolecules. *Biosens. Bioelectron.* **2016**, *86*, 432−438.
(28) Li, J.; Zhao, J.; Li, S.; Chen, Y.; Lv, W.; Zhang, J.; Zhang, L.; Zhang, Z.; Lu, X. Synergistic Effect Enhances the Peroxidase-Like Activity in Platinum Nanoparticle-Supported Metal-Organic Framework Hybrid Nanozymes for Ultrasensitive Detection of Glucose. *Nano Res.* **2021**, *14*, 4689−4695.
(29) Ren, G.; Dong, F.; Zhao, Z.; Li, K.; Lin, Y. Structure Defect Tuning of Metal-Organic Frameworks as a Nanozyme Regulatory Strategy for Selective Online Electrochemical Analysis of Uric Acid. *ACS Appl. Mater. Interfaces* **2021**, *13*, 52987−52997.
(30) Lu, Z.; Dang, Y.; Dai, C.; Zhang, Y.; Zou, P.; Du, H.; Zhang, Y.; Sun, M.; Rao, H.; Wang, Y. Hollow MnFeO Oxide Derived from MOF@MOF with Multiple Enzyme-Like Activities for Multifunction Colorimetric Assay of Biomolecules and Hg^{2+}. *J. Hazard. Mater.* **2021**, *403*, 123979−123988.
(31) Luo, L.; Huang, L.; Liu, X.; Zhang, W.; Yao, X.; Dou, L.; Zhang, X.; Nian, Y.; Sun, J.; Wang, J. Mixed-Valence Ce-BPyDC Metal-Organic Framework with Dual Enzyme-like Activities for Colorimetric Biosensing. *Inorg. Chem.* **2019**, *58*, 11382−11388.
(32) Jureviciute, I.; Jackson, A.; Hillman, A. R.; Bruckenstein, S. Redox History Effects Accompanying the Electrochemical Cycling of Poly(vinylferrocene). *J. Solid State Electrochem.* **2004**, *8*, 403−410.
(33) Bloksma, A. H. Oxidation by Potassium Iodate of Thiol Groups in Unleavened Wheat Flour Doughs. *J. Sci. Food Agric.* **1964**, *15*, 83−94.
(34) Ran, Y.; Yang, Y.; Zhang, L. Sodium Chlorate as a Viable Substoichiometric Oxidant for Cobalt-Catalyzed Oxidative Annulation of Aryl Sulfonamides with Alkynes. *Tetrahedron Lett.* **2016**, *57*, 3322−3325.
(35) Chen, K.; Wu, C. D. Transformation of Metal-Organic Frameworks into Stable Organic Frameworks with Inherited Skeletons and Catalytic Properties. *Angew. Chem., Int. Ed.* **2019**, *58*, 8119−8123.
(36) Liu, H.; Wang, L.; Wang, X.; Hu, Y.; Feng, L.; Dong, S.; Hao, J. Vesicle Transition of Catanionic Redox-Switchable Surfactants Controlled by DNA with Different Chain Lengths. *J. Colloid Interface Sci.* **2019**, *549*, 89−97.
(37) Ahmed, S.; Chatterjee, A.; Das, K.; Das, D. Fatty Acid Based Transient Nanostructures for Temporal Regulation of Artificial Peroxidase Activity. *Chem. Sci.* **2019**, *10*, 7574−7578.
(38) Saji, T.; Hoshino, K.; Ishii, Y.; Goto, M. Formation of Organic Thin Films by Electrolysis of Surfactants with the Ferrocenyl Moiety. *J. Am. Chem. Soc.* **1991**, *113*, 450−456.
(39) Attah-Kyei, D.; Klemettinen, L.; Michallik, R.; Salminen, J.; Taskinen, P.; Lindberg, D. Hydrogen as Carbon-Free Reducing Agent in Non-ferrous Slag Fuming. *Metall. Mater. Trans. B* **2022**, *53*, 3775−3792.
(40) Chen, L.; Yang, J.; Suh, B. I. Effect of Oxidizing Agents on Bond of New Self-Adhesive Cement. *Dent. Mater.* **2018**, *34*, e26−e27.
(41) Eseva, E. A.; Akopyan, A. V.; Anisimov, A. V.; Maksimov, A. L. Oxidative Desulfurization of Hydrocarbon Feedstock Using Oxygen as Oxidizing Agent (a Review). *Pet. Chem.* **2020**, *60*, 979−990.
(42) Palomba, M.; Carotenuto, G.; Longo, A. A Brief Review: The Use of L-Ascorbic Acid as a Green Reducing Agent of Graphene Oxide. *Mater.* **2022**, *15*, 6456−6471.
(43) Pesti, J.; Larson, G. L. Tetramethyldisiloxane: A Practical Organosilane Reducing Agent. *Org. Process Res. Dev.* **2016**, *20*, 1164−1181.
(44) Siahrostami, S.; Villegas, S. J.; Bagherzadeh Mostaghimi, A. H.; Back, S.; Farimani, A. B.; Wang, H.; Persson, K. A.; Montoya, J. A Review on Challenges and Successes in Atomic-Scale Design of Catalysts for Electrochemical Synthesis of Hydrogen Peroxide. *ACS Catal.* **2020**, *10*, 7495−7511.
(45) Yentekakis, I. V.; Georgiadis, A. G.; Drosou, C.; Charisiou, N. D.; Goula, M. A. Selective Catalytic Reduction of NO_x over Perovskite-Based Catalysts Using $C_xH_y(O_z)$, H_2 and CO as Reducing Agents-A Review of the Latest Developments. *Nanomaterials* **2022**, *12*, 1042−1076.
(46) Mahmoud, W. H.; Omar, M. M.; Ahmed, Y. M.; Mohamed, G. G. Transition Metal Complexes of Schiff Base Ligand Based on 4,6-Diacetyl Resorcinol. *Appl. Organometal Chem.* **2020**, *34*, No. e5528.
(47) Gallardo, B. S.; Metcalfe, K. L.; Abbott, N. L. Ferrocenyl Surfactants at the Surface of Water: Principles for Active Control of Interfacial Properties. *Langmuir* **1996**, *12*, 4116−4124.
(48) Chang, Y.; Yang, K.; Wei, P.; Huang, S.; Pei, Y.; Zhao, W.; Pei, Z. Cationic Vesicles Based on Amphiphilic Pillar[5]arene Capped with Ferrocenium: A Redox-responsive System for Drug/siRNA Co-Delivery. *Angew. Chem., Int. Ed.* **2014**, *53*, 13126−13130.
(49) Estévez-Torres, A.; Baigl, D. DNA Compaction: Fundamentals and Applications. *Soft Matter* **2011**, *7*, 6746−6756.
(50) Bhattacharjee, S. DLS and zeta potential - What they are and what they are not? *J. Controlled Release* **2016**, *235*, 337−351.

https://doi.org/10.1021/acsomega.4c01715
ACS Omega 2024, 9, 23772−23781